Recognition and Activation of Rho GTPases by Vav1 and Vav2 Guanine Nucleotide Exchange Factors †

ARTICLE *in* BIOCHEMISTRY · JUNE 2005

Impact Factor: 3.02 · DOI: 10.1021/bi047443q · Source: PubMed

3 AUTHORS, INCLUDING:

Roopa Thapar
University of Texas MD Anderson Cancer Center
28 PUBLICATIONS **395** CITATIONS
SEE PROFILE

Sharon l Campbell
University of North Carolina at Chapel Hill
104 PUBLICATIONS **5,406** CITATIONS
SEE PROFILE

Recognition and Activation of Rho GTPases by Vav1 and Vav2 Guanine Nucleotide Exchange Factors†

Jongyun Heo,‡ Roopa Thapar,‡ and Sharon L. Campbell*,‡,§

Department of Biochemistry and Biophysics and Lineberger Comprehensive Cancer Center, University of North Carolina, 530 Mary Ellen Jones Building, Chapel Hill, North Carolina 27599-7260

Received December 6, 2004; Revised Manuscript Received February 21, 2005

ABSTRACT: Vav proteins are Rho GTPase-specific guanine nucleotide exchange factors (GEFs) that are distinguished by the tandem arrangement of Dbl homology (DH), Pleckstrin homology (PH), and cysteine rich domains (CRD). Whereas the tandem DH−PH arrangement is conserved among Rho GEFs, the presence of the CRD is unique to Vav family members and is required for efficient nucleotide exchange. We provide evidence that Vav2-mediated nucleotide exchange of Rho GTPases follows the Theorell−Chance mechanism in which the Vav2•Rho GTPase complex is the major species during the exchange process and the Vav2•GDP-Mg^{2+}•Rho GTPase ternary complex is present only transiently. The GTPase specificity for the DH−PH−CRD Vav2 in vitro follows this order: Rac1 > Cdc42 > RhoA. Results obtained from fluorescence anisotropy and NMR chemical shift mapping experiments indicate that the isolated Vav1 CRD is capable of directly associating with Rac1, and residues K116 and S83 that are in the proximity of the P-loop and the guanine base either are part of this binding interface or undergo a conformational change in response to CRD binding. The NMR studies are supported by kinetic measurements on Rac1 mutants S83A, K116A, and K116Q and Vav2 CRD mutant K533A in that these mutants affect both the initial binding event of Vav2 with Rac1 (k_{on}) and the rate-limiting dissociation of Vav2 from the Vav2•Rac1 binary complex (thereby influencing the enzyme turnover number, k_{cat}). The results suggest that the CRD domain in Vav proteins plays an active role, affecting both the k_{on} and the k_{cat} for Vav-mediated nucleotide exchange on Rho GTPases.

Rho GTPases have emerged as key regulators in the control of cell differentiation and proliferation, cell motility, cell adhesion, gene expression, transformation, apoptosis, phagocytosis, and the cell cycle (*1*−*3*). Like Ras, Rho proteins function as molecular switches, and cycle between their active GTP-bound and inactive GDP-bound states (*4*−*7*). Given their roles in cellular growth control, there is a great deal of interest in understanding the mechanism by which Rho GTPases are activated and regulated.

For most Rho proteins, the exchange of GDP for GTP is accelerated by members of the Dbl family of guanine nucleotide exchange factors (GEFs)[1] (*4*−*9*). There are now more than 30 mammalian members of the Dbl family of GEFs, and these proteins are characterized by the tandem arrangement of a conserved catalytic Dbl homology (DH) domain N-terminal to a Pleckstrin homology (PH) domain. Recent crystallographic structures of Rac1−Tiam1 DH−PH (*10*), Cdc42−Dbs DH−PH (*11*), Cdc42−Intersectin DH−PH, and RhoA−Dbs DH−PH (*12*) complexes along with biochemical evidence from site-directed mutagenesis (*13*−*15*) reveal that a critical helix, α_5 (Tiam1 numbering), along with the three helices that make up the conserved regions of the DH domain, recognizes residues in the two switch regions of the GTPase in a lock-and-key fashion. These studies suggest that the DH domain is essential for GNE activity such that the binding of the DH domain to the GTPase leads to a conformational change in the nucleotide-binding pocket which particularly affects the switch 2 region (residues 59−67), resulting in perturbation of the Mg^{2+}-binding site near A59 and the loss of a key K16−GDP β-phosphate interaction. The conserved PH domain of Dbl family proteins is known to be involved in protein−protein and protein−lipid interactions that may regulate the function of the DH domain (*16*, *17*).

The Vav[2] family of proteins are a subfamily of the Dbl family of GEFs and exhibit substrate specificity toward a number of Rho GTPases (RhoA, RhoB, RhoG, Rac1, and Cdc42) in vitro and in vivo (*17*−*19*). All Vav proteins (Vav1, Vav2, Vav3, *Drosophila* Vav, and *Caenorhabditis elegans* Vav) have a number of highly conserved protein−protein and protein−lipid interaction domains, including a DH−PH bidomain (*4*, *20*). As in other Dbl family GEFs, the DH domain of Vav1, Vav2, and Vav3 promotes GNE on Rho GTPases (*16*, *17*). However, the mechanism of Vav DH-mediated Rho GTPase GNE has not been fully elucidated.

† This work was supported by NIH Grant RO1CA89614-O1A1 to S.L.C. and Grant R01CA83943-01 to S.L.C. and R.T.

* To whom correspondence should be addressed. E-mail: campbesl@med.unc.edu. Fax: (919) 966-2852. Telephone: (919) 966−7139.

‡ Department of Biochemistry and Biophysics.

§ Lineberger Comprehensive Cancer Center.

[1] Abbreviations: GEFs, guanine nucleotide exchange factors; GNE, guanine nucleotide exchange; GMPPNP, guanosine 5′-(β,γ-imido)-triphosphate; PMSF, phenylmethanesulfonyl fluoride; NMR, nuclear magnetic resonance; HSQC, heteronuclear single-quantum coherence; DH, Dbl homology; PH domain, Pleckstrin homology domain; CRD, cysteine-rich domain; DPC, Vav protein containing DH, PH, and CRD domains; SD, standard deviation.

10.1021/bi047443q CCC: $30.25
Published on Web 04/08/2005

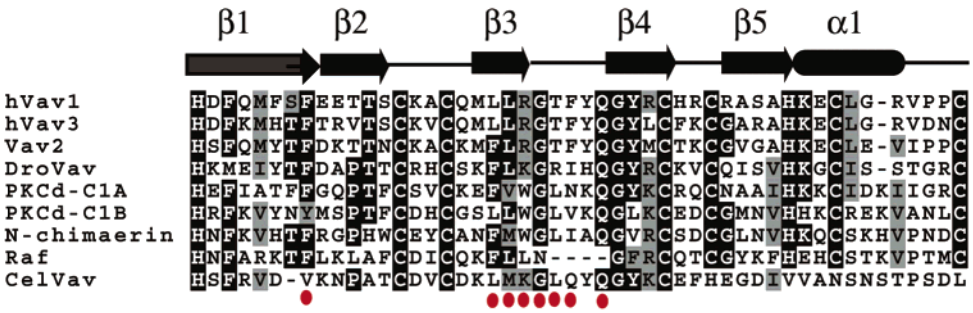

FIGURE 1: Multiple-sequence alignment of cysteine-rich domains shared by the Vav family of GEFs. Vav1 and Vav2 are the most closely related members within the Vav subfamily, and the sequences of their CRDs are 62% identical and 72% similar. The multiple-sequence alignment of the Vav1 and Vav2 CRDs with the CRDs from the atypical CRD of Raf-1 and that of the DAG-binding CRD of PKC-δ is shown. The locations of β-strands and the C-terminal helix were obtained from the NMR structure of the Raf-1 CRD (PDB entries 1FAQ and 1FAR) as designated above. Residues that are important for diacylglycerol and membrane binding in the typical CRDs, based upon the PKC-δ crystal structures (PDB entries 1PTQ and 1PTR), are highlighted with red circles. These residues are not strictly conserved in the CRD of the Vav subfamily or in the Raf kinase CRD, neither of which binds phorbol esters or DAG. The last two zinc-coordinating cysteines are missing in *C. elegans* Vav, suggesting that the CRD will either not fold properly or adopt a similar fold; however, the significance of the difference in the CRD in *C. elegans* compared to other Vav members remains unclear.

While the DH domain of Vav1, Vav2, and Vav3 is essential for facilitating GNE on Rho GTPases, Vav family GEFs also have an additional cysteine-rich domain (CRD, also termed the C1 domain) C-terminal to the DH−PH bidomain (*16*, *17*). In Vav1 and Vav2, the PH domains are known to bind the products and substrates of PI 3-kinase such as phosphatidylinositol 4,5-biphosphate (PIP_2) and phosphatidylinositol 3,4,5-triphosphate (PIP_3) (*21*). These phosphoinositides have previously been shown to regulate Vav GEF activity (*21*). In addition, the CRD of Vav1 and Vav2 can also directly modulate GEF activity in the absence of a membrane environment or phospholipids (*16*−*18*), suggesting a distinct role for this domain in promoting GNE on Rho GTPases. The molecular basis for this regulation remains to be elucidated.

The kinetic results presented herein provide insight into the mechanism of Vav1- and Vav2-mediated GNE on Rho family GTPases. A multidisciplinary approach, including fluorescence anisotropy, NMR-based chemical shift mapping, and kinetic measurements, has been employed to elucidate the role of the CRD in DH-mediated Rho GTPase GNE catalyzed by Vav proteins.

MATERIALS AND METHODS

The chemicals used for all experiments were of the highest grade unless otherwise documented. 2′(3′)-*O*-(*N*-Methylanthraniloyl)guanosine 5′-diphosphate (mant-GDP) was purchased from Molecular Probes. The mant-GDP-Mg^{2+} assay mixture consists of 0.1 mM mant-GDP, 0.9 mM unlabeled GDP, 5 mM $MgCl_2$, and guanine nucleotide exchange assay buffer (GNE assay buffer). The GNE assay buffer contains 10 mM $MgCl_2$, 50 mM NaCl, and 20 mM Tris-HCl (pH 7.5).

Protein Sample Preparation. The GTPases Rac1(1−177), Cdc42(1−188), and RhoA(1−181) were expressed and purified as described previously (*17*). The final purities of the proteins were >95% as determined by SDS−PAGE. Protein concentrations were determined by the Bradford method (*22*).

The Vav CRD constructs span residues 514−566 of Vav1 and residues 522−573 of Vav2 (Figure 1). These regions encompass the structural limits of the Raf kinase (*23*) and PKCδ (*24*) CRD domains for which NMR solution and crystal structures are available. The Vav1 and Vav2 CRDs and the Vav1 PH−CRD are not stably expressed as individual domains in *Escherichia coli*, and upon cleavage from a fused N-terminal maltose-binding protein (MBP) tag, these constructs tend to be insoluble. However, when expressed as a MBP fusion protein, both the Vav1 CRD and the Vav1 PH−CRD are soluble. Therefore, the Vav1 CRD was expressed as an MBP fusion protein from vector pMAL (NEB) as described by the manufacturer. The Factor Xa site of pMAL was re-engineered into a thrombin cleavage site. However, since the Vav1 CRD was insoluble after thrombin cleavage, the MBP was left as a solubility enhancement tag for all NMR experiments. MBP alone was also expressed and purified from the same vector and used as a control. In addition to the Vav1 MBP−CRD and Vav1 MBP−PH−CRD proteins, we also expressed the Vav1 MBP−DH−PH−CRD protein. However, unlike the Vav2 DH−PH−CRD (Vav2 DPC) protein which is highly active in fluorescence-based Rho GTPase GNE assays, the Vav1 DH−PH−CRD protein (Vav1 DPC) is not. This is consistent with previous studies (*25*) in which a very high concentration (50-fold molar excess) of the Vav1 DH domain was required relative to the Rac1 GTPase for efficient Vav1-mediated GNE. At these ratios, no measurable GNE activity was detected toward Cdc42 and RhoA GTPases (*25*). In contrast to Vav1, we require only catalytic amounts of the Vav2 DH−PH−CRD

[2] Although traditionally the term Vav has been used to refer to Vav1, for the sake of simplicity we have used the term "Vav" to refer to the Vav family of proteins in general. When referring to a particular Vav isoform, we specify Vav1 or Vav2. In this study, we present kinetic results on various forms of Vav (Vav DH and Vav DH−PH−CRD), Vav substrates (Rho GTPases, Rac1, Rac1 mutants, Cdc42, and RhoA), and ligand GNPs (GDP and GMPPNP). To simplify the description of the kinetic parameters, we have employed an abbreviated notation. For example, the apparent dissociation constant (K_D) describing interactions of the Vav2 DH domain with Rac1 is represented as ${}^{app}K_{D(Vav2\ DH-Rac1)}$, where the superscript app on the left side of K_D denotes that this is an apparent equilibrium rate constant. Moreover, the subscripted notation Vav2 DH−Rac1 within parentheses on the right side of K_D indicates that the Vav2 DH domain is an enzyme while Rac1 is a substrate. Similarly, the true dissociation constant of Rac1 for its GDP-Mg^{2+} ligand is depicted as ${}^{true}K_{D(Rac1-GDP)}$, where the superscripted true on the left side of K_D denotes that the constant is not apparent. The subscripted notation Rac1−GDP within the parentheses on the right side of K_D indicates that GDP is a ligand of Rac1.

Table 1: Comparison of Kinetic Values[a]

		Rac1					
		wild type	S83A	K116A	K116Q	Cdc42	RhoA
Vav2 DH	$V_{max(Vav2\ DH-GTPase)}$	$(0.03 \pm 0.01) \times 10^5$	480 ± 76	21 ± 4	13 ± 6	160 ± 34	14 ± 4
	$k_{cat(Vav2\ DH-GTPase)}$	0.6×10^6	0.1×10^6	4200	2600	32000	2800
	$K_{M(Vav2\ DH-GTPase)}$	5.1 ± 1.6	5.8 ± 0.7	6.4 ± 0.8	8.1 ± 0.7	9.5 ± 3.0	7.8 ± 2.0
Vav2 DPC	$V_{max(Vav2\ DPC-GTPase)}$	$(0.12 \pm 0.01) \times 10^5$	$(0.03 \pm 0.01) \times 10^5$	163 ± 13	150 ± 3	430 ± 30	19 ± 2
	$k_{cat(Vav2\ DPC-GTPase)}$	12.9×10^6	0.6×10^6	32600	30000	86000	3800
	$K_{M(Vav2\ DPC-GTPase)}$	5.1 ± 0.8	7.3 ± 1.2	8.2 ± 0.7	9.0 ± 0.4	5.9 ± 1.2	7.2 ± 1.7
Vav2 DPC K533A	$V_{max(Vav2\ DPC\ K533A-GTPase)}$	$(0.05 \pm 0.02) \times 10^5$	590 ± 53	24 ± 12	36 ± 15	320 ± 96	32 ± 6
	$k_{cat(Vav2\ DPC\ K533A-GTPase)}$	3.8×10^6	0.5×10^6	12900	21700	63000	3400
	$K_{M(Vav2\ DPC\ K533A-GTPase)}$	11.5 ± 1.8	12.9 ± 4.9	13.4 ± 5.0	11.3 ± 4.7	12.3 ± 3.6	11.5 ± 6.9

[a] The kinetic values V_{max} (μM GDP-Mg^{2+} min^{-1}) and K_M (μM GDP-Mg^{2+}) are obtained (Figures 1 and 2 of the Supporting Information), but with different combinations of Vav2 enzymes (Vav2 DH, Vav2 DPC, and Vav2 DPC K533A) and GTPase substrates (Rac1, Rac1 S83A, Rac1 K116A, Rac1 K116Q, Cdc42, and RhoA). A catalytic amount of either the Vav2 DH or Vav2 DPC enzyme (10−50 nM) was used for all GTPase activity assays. The k_{cat} (min^{-1}) values were estimated using eq 3 of the Supporting Information. The values presented in this table are the result of the best fit ($r^2 > 0.8065$) to a simple hyperbola with the corresponding SD.

protein such that GNE is observed at molar ratios of 1.000:0.005 (GTPase:Vav2). Therefore, all kinetic measurements were conducted in the context of the Vav2 protein. The sequence of Vav3 CRD is 71% and 61% identical the Vav1 and Vav2 CRDs, respectively, and the Vav3 CRD has been reported to bind directly to RhoA (*26*). Given the high level of sequence identify among the Vav CRDs (sequences of Vav1 and Vav2 CRDs are 62% identical), the general mode of association of the Vav family of CRD domains with Rho GTPases is likely to be similar. The final purities of the proteins were >95% as determined by SDS−PAGE. Protein concentrations were determined by the Bradford method (*22*).

Determination of Kinetic Parameters for Vav2-Mediated GTPase Guanine Nucleotide Exchange. The kinetic data were collected under conditions where the ligand and/or substrate was present under saturating conditions; i.e., the concentration of the GDP-Mg^{2+} ligand (e.g., 1 mM) is in excess over the dissociation constant of GDP-Mg^{2+} for the Rho GTPase (*27*, *28*). These experimental conditions mimic saturation conditions that are likely to occur in vivo, as nucleotide (i.e., GTP) levels are present in excess of GTPase (*29*). Quantitative kinetic values for Vav2-mediated GTPase GNE were estimated using fluorescence-based approaches employing fluorescent mant-labeled GDP (mant-GDP-Mg^{2+}) and measuring kinetics of mant-GDP association and dissociation from Rac1, RhoA, and Cdc42 GTPases (*30*) (details in the Supporting Information). The kinetic values measured in these experiments include Vav2 catalytic activity (μM mant-GDP-Mg^{2+} exchanged min^{-1}), the specific activity of Vav2 [μM GDP-Mg^{2+} exchanged min^{-1} (mg of Vav2)$^{-1}$], the Henri−Michaelis−Menten constant of Vav2 for the GTPase [$K_{M(Vav2-GTPase)}$], the maximum velocity [$V_{max(Vav2-GTPase)}$], and rate-limiting rate constant (k_{cat}) of Vav2 for the GTPases (*27*). Binding constants for the GTPase·Vav2 binary complex (the true dissociation constants of Vav2 for the GTPase [$^{true}K_{D(Vav2-GTPase)}$]) were determined using two independent approaches: a fluorescence mant-GDP-based assay (method I) and a tryptophan fluorescence-based assay (method II) (details in the Supporting Information). Rate constants for Vav2-mediated GNE on various Rho family GTPases were determined from the $^{true}K_{D(Vav2-GTPase)}$, $K_{M(Vav2-GTPase)}$, and k_{cat} (details in the Supporting Information).

Apparent equilibrium dissociation constants for the Vav1 MBP−CRD and Vav1 MBP−PH−CRD proteins with Rac 1 and RhoA GTPases [$^{Vav1\ app}K_{D(MBP-CRD-GTPase\cdot GNP)}$ and $^{Vav1app}K_{D(MBP-PH-CRD-GTPase\cdot GNP)}$] were determined by fluorescence anisotropy using mant-GDP and mant-GMPPNP (a nonhydrolyzable analogue of GTP) (details in the Supporting Information).

NMR Sample Preparation. NMR samples used for chemical shift mapping experiments contained uniformly ^{15}N-labeled Rac1*dm* GTPase (residues 1−188 with the C178S mutation) and unlabeled MBP−CRD or MBP in 50 mM Tris-maleate buffer, 50 mM NaCl, 100 μM GDP, 20 mM $MgCl_2$, 10 mM DTT, and 0.1% sodium azide at pH 6.8 in a 9:1 $H_2O/^2H_2O$ mixture. The expression, purification, solution behavior, and spectral characteristics of the Rac1*dm* isoform have been described elsewhere (*31*). $^1H-^{15}N$ HSQC spectra were acquired for MBP−Vav1 CRD:Rac1*dm* and MBP:Rac1*dm* molar ratios (as a control) of 1.0:1.0, 1.0:0.5, and 1.0:0.0. The starting concentration of ^{15}N-labeled Rac1 and unlabeled MBP or MBP−CRD was 0.25 mM. Serial dilutions were made by exchanging equal volumes of the Rac1−MBP complex with the starting stock solution of free Rac1.

NMR Data Acquisition and Processing. NMR data were collected at 35 °C on an Inova 600 MHz spectrometer equipped with a 5 mm *z*-gradient triple-resonance probe. Two-dimensional $^1H-^{15}N$ gradient sensitivity-enhanced HSQC spectra were acquired with 64 transients per t_1 increment and 256 t_1s. Spectra were processed using Felix 98.2 (Accelrys).

RESULTS

Kinetic Comparison of Vav2-Mediated GNE of RhoA, Rac1, and Cdc42. It has been previously shown that Vav2 can facilitate GNE on the GTPases Rac1, Cdc42, and RhoA in vitro and in vivo (*18*, *19*, *32*, *33*). However, a detailed kinetic analysis of these GTPases with Vav2 has not been performed. Since the Dbl homology domain of Vav2 (Vav2 DH) is considered to be the minimal functional domain responsible for GNE of Rho GTPases, kinetic parameters were initially determined for Vav2 DH-mediated Rho GTPase GNE. Table 1 shows a comparison of the V_{max} and K_M values of the Vav2 DH domain for various Rho GTPase substrates. Intriguingly, although the K_M values of the Vav2 DH for RhoA, Rac1, and Cdc42 are similar, the V_{max} values are quite variable such that the V_{max} for Rac1 is ~20- and ~200-fold larger than that for Cdc42 and RhoA, respectively.

Scheme 1

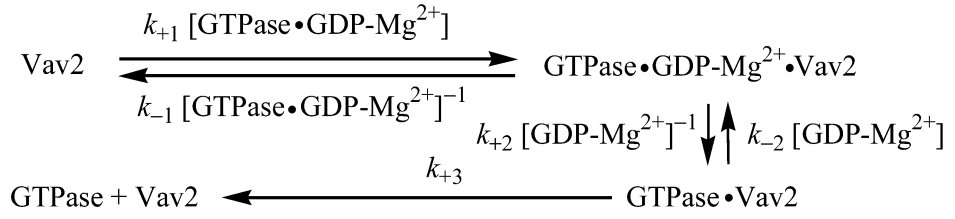

V_{max} can be converted to k_{cat}, the rate-limiting turnover number for the overall enzymatic process, according to eq 3 of the Supporting Information. It is noteworthy that the differences in k_{cat} values of Vav2 DH for Rho GTPases were identical to that of V_{max}, since the same amount of Vav2 DH was used in all assays (Table 1). While k_{cat} values are variable for each Rho GTPase substrate, the K_M values are similar, indicating that the relative catalytic efficiency (k_{cat}/K_M) (*34*) of Vav2 DH for Rho GTPases is primarily dictated by the k_{cat}. Therefore, the rank order of catalytic efficiency in our kinetic studies is as follows: Rac1 ≫ Cdc42 > RhoA (relative ratios: ∼200 ≫ ∼10 > 1). This result suggests that, at least for the minimal DH−PH−CRD unit and in the absence of post-translational modifications, Rac1 may be the preferred substrate for Vav2. The overall catalytic efficiency was greatly increased when the DH construct was extended to include the CRD domain (DPC), yet the rank order of catalytic efficiency paralleled that of the Vav2 DH domain alone (Rac1 ≫ Cdc42 > RhoA; relative ratios: ∼4600 ≫ ∼30 > 1) (Table 1) [again, the ratio comparison was made by setting the k_{cat} of Vav2 DH for RhoA (2800 min^{-1}) equal to 1].

The Interaction of Vav2 DPC with Rac1 Follows the Theorell−Chance Mechanism. Evidence from crystallographic (*10*, *12*, *35*) and kinetic measurements shows that Rho GEFs interact with Rho GTPases at two sites, namely, the Mg^{2+}-binding site (primarily in the switch I region) and the guanine nucleotide-binding site (both switches I and II) (*36*). Zhang et al. showed that the Rho GEF (Trio) decreases the Rho GTPase Rac1−Mg^{2+} binding affinity significantly (*36*). More recently, kinetic studies showed a two-step process for Rho GTPase Rac GNE, whereby Mg^{2+} is released first followed by dissociation of the nucleotide (*37*). Intriguingly, the Mg^{2+}-free GDP-bound structure of RhoA shows a large conformational change only in the switch I region of RhoA, but not the RhoA nucleotide-binding site (*38*). These results, when taken together (*36*−*38*), indicate that Rho GEFs perturb both the Mg^{2+}-binding site and the nucleotide-binding site of Rho GTPases. However, disruption of Mg^{2+} binding appears to be the dominant effect on the rate-limiting catalytic step k_{cat}. Thus, when a Rho GEF binds to a Rho GTPase•GDP-Mg^{2+} complex, the first step may involve release of Mg^{2+} and the rate of release of bound nucleotide from the GTPase may be rate-determining (*36*, *37*). In this case, a Mg^{2+}-free GTPase•GDP•GEF complex should be observable, wherein the GTPase•GDP•GEF complex reflects interactions between the GEF and the Mg^{2+} site of the Rho GTPase (the complex therefore lacks "Mg^{2+}") but not the guanine nucleotide site of the GTPase. In our kinetic models (vide infra, Schemes 1 and 2), Vav-mediated exchange of guanine nucleotide and exchange Mg^{2+} are not described as separate events. It is difficult to use equilibrium measurements such as those employed herein to dissect the two

Scheme 2

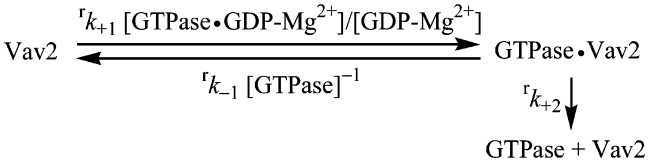

microscopic rate constants for these processes because they may be coupled. The interaction of the GEF with the Mg^{2+}-binding site of the Rho GTPase influences the interaction of GTPase with the nucleotide (which lacks Mg^{2+}) (*36*, *37*). Therefore, we treat the nucleotide, GDP, and Mg^{2+} as a single molecule (GDP-Mg^{2+}). Moreover, the GTPase•GDP-Mg^{2+}•Vav2 complex is described as a ternary complex of GTPase, GDP-Mg^{2+}, and GEF. We use this notation throughout the paper.

The catalytic mechanism proposed for Vav2-mediated GNE of Rho GTPases is described in Scheme 1, and is based on previous mechanistic studies of the Ras GTPase with its GEF, Cdc25 (*39*).

In Scheme 1, the GTPase•GDP-Mg^{2+}•Vav2 ternary complex is formed first, followed by the release of GDP-Mg^{2+} to generate the GTPase•Vav2 binary complex. The binary complex dissociates to a GDP-deficient form of the GTPase (apo-GTPase) and free Vav2. The apo-GTPase can then rebind either GDP-Mg^{2+} or Vav2. Therefore, at equilibrium, the GTPase, GDP-Mg^{2+}, and Vav2 could be present as GTPase•GDP-Mg^{2+} binary, GTPase•Vav2 binary, and GTPase•GDP-Mg^{2+}•Vav2 ternary complexes. The relative populations of these individual components depend on the individual equilibrium of the enzymatic reaction components, as shown in eq 4 of the Supporting Information.

To determine the relative populations of these complexes at equilibrium, the Rac1•GDP-Mg^{2+} complex was titrated with increasing amounts of the Vav2 DH domain, and the formation of Rac1•Vav2 DH complexes was monitored using the intrinsic Rac1 W56 and W97 fluorescence. An increase in the intrinsic tryptophan fluorescence (data not shown) was observed upon titration of the Vav2 DH into Rac1, suggesting that the titration produced either the Rac1•GDP-Mg^{2+}•Vav2 DH ternary or Rac1•Vav2 DH binary complex. To determine whether the Rac1•GDP-Mg^{2+}•Vav2 ternary complex is long-lived (Scheme 1), an alternative approach was employed. The fluorescent mant-GDP analogue was loaded onto Rac1 in the presence of Mg^{2+} to produce a Rac1•mant-GDP-Mg^{2+} binary complex, and the mant-GDP-loaded Rac1 complex was titrated with Vav2 DH at saturating levels of GDP and Mg^{2+} (5 mM) to force the formation of the Rac1•mant-GDP-Mg^{2+}•Vav2 DH ternary complex (Figure 3). As shown in Figure 3, the mant-GDP fluorescence intensity decreased in response to the addition of the Vav2 DH domain, indicating that mant-GDP-Mg^{2+} is released from Rac1. If mant-GDP-

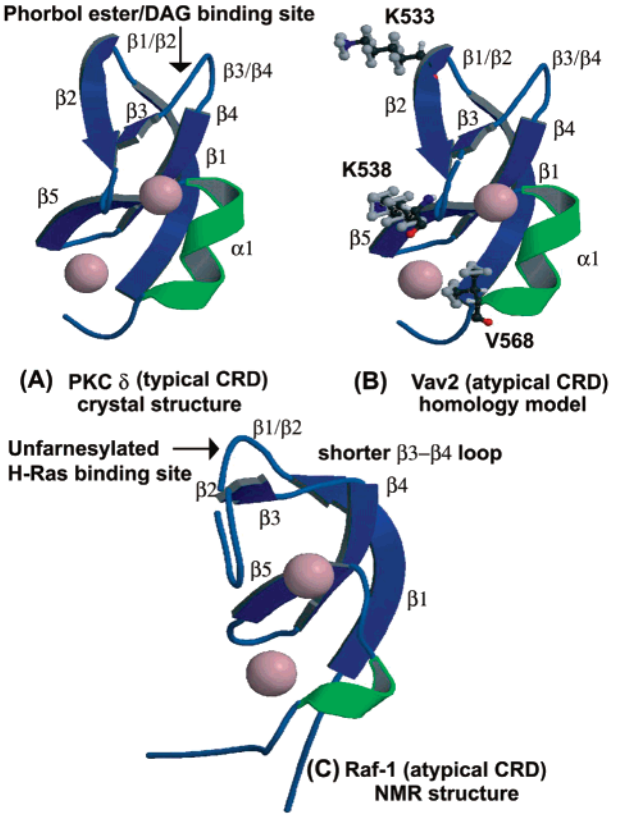

FIGURE 2: Comparison of the cysteine-rich domains from PKC-δ, Vav2, and Raf-1 kinase. The crystal structure of the "typical" phorbol ester and DAG binding C1 domain (or CRD) from PKC-δ C1A (PDB entry 1PTQ) is compared to the NMR structure of the "atypical" CRD from Raf-1 kinase (PDB entry 1FAR). The Raf-1 kinase CRD is not known to bind phorbol esters and DAG, and correspondingly, the $\beta1-\beta2$ and $\beta3-\beta4$ loops are smaller and not hydrophobic as observed in the typical CRDs. Instead, they are rich in charged amino acids that are known to bind unfarnesylated H-Ras. Similar to the typical CRDs, the Vav family has a longer $\beta3-\beta4$ loop that is also rich in hydrophobic amino acids, although so far the Vav2 CRD is not reported to bind phorbol esters or DAG. A homology model of the Vav2 CRD was constructed as described in the Supporting Information to define the orientation of residues K533, K538, and V568 that were previously (*17*) shown to be important for Vav2 function in vivo. The model is compared to the NMR structure of the Raf-1 CRD (PDB entry 1FAR) and the crystal structure of the PKC-γ C1b (PDB entry 1TBN). It shows an overall structure similar to that of the typical CRDs, and both K533 and K538 are solvent-exposed and available for molecular recognition with either phosphoinositide or GTPase substrates. The side chain of V568 may be necessary for stabilization of the CRD.

Mg^{2+} were not released from Rac1, the Rac1·mant-GDP-Mg^{2+}·Vav2 DH ternary complex would be formed during the titration, and a decrease in mant fluorescence intensity would not be observed. The release of mant-GDP-Mg^{2+} is immediate, suggesting that the reaction approaches equilibrium rapidly under our experimental conditions. Using eq 1 of the Supporting Information, the fraction of mant-GDP released can be calculated, and was found to be equivalent to the amount of the titrant Vav2 DH, indicating that addition of Vav2 DH to the Rac1·mant-GDP-Mg^{2+} binary complex results in a nearly 1:1 stoichiometric displacement of Rac1-bound mant-GDP-Mg^{2+} with Vav2 DH to produce the Rac1·Vav2 DH binary complex. As summarized in Table 2, when Cdc42 and RhoA were titrated with Vav2 DH under identical experimental conditions, the binary Cdc42·Vav2 DH and RhoA·Vav2 DH complexes were also observed. Similar

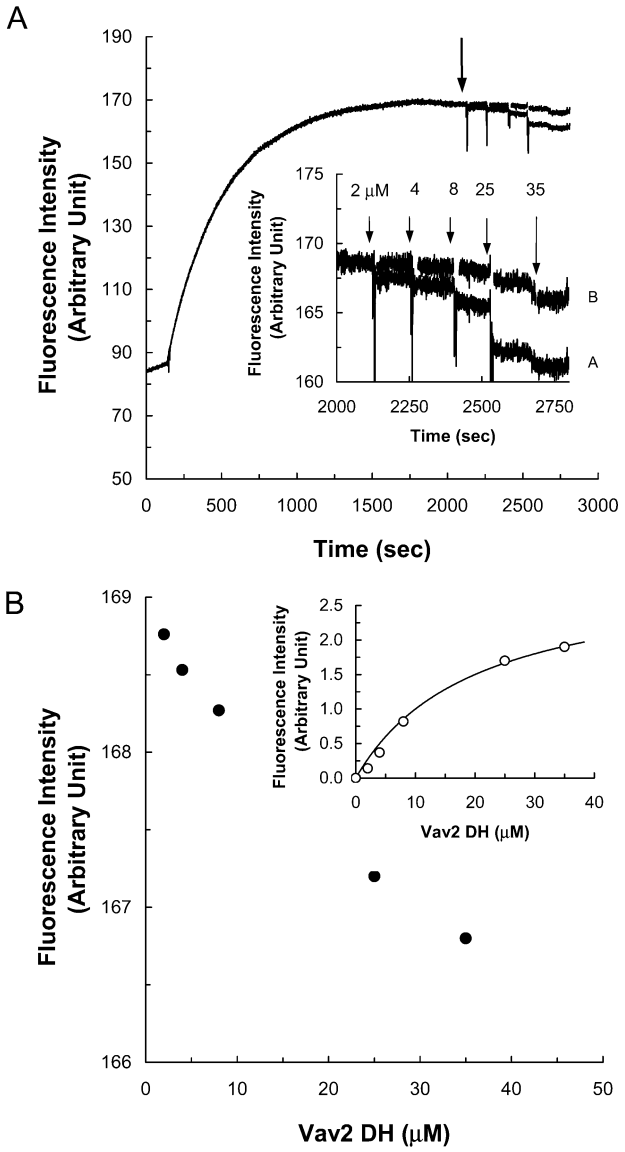

FIGURE 3: Fluorescence mant-GDP-based determination of dissociation constants for the GTPase·Vav2 DH binary complex (method I). (A) Rac1 (1.0 μM) was placed in GNE assay buffer containing the mant-GDP-Mg^{2+} mixture (1 mM). A catalytic amount of the Vav2 DPC (1 nM) was added to facilitate exchange of Rac1-bound GDP-Mg^{2+} with mant-GDP-Mg^{2+}. Once the Rac1-bound mant-GDP-Mg^{2+} and free mant-GDP-Mg^{2+} reach equilibrium as indicated by the arrow, mant-GDP-Mg^{2+}-bound Rac1 is titrated with the Vav2 DH domain and the corresponding changes in fluorescence intensity are monitored. (B) Change in fluorescence intensity due to the dissociation of mant-GDP-Mg^{2+} from Rac1 caused by the formation of the Rac1·Vav2 DH binary complex plotted against the Vav2 DH domain concentration. The plot was fit to a simple hyperbola to obtain ${}^{app}K_{D(Vav2\ DH-Rac1)}$. The ${}^{app}K_{D(Vav2\ DH-Rac1)}$ was converted to a ${}^{true}K_{D(Vav2\ DH-Rac1)}$ using eq 6 of the Supporting Information. This compensation and conversion gave a ${}^{true}K_D$ value of Rac1 for the Vav2 DH domain (0.09 ± 0.04 μM Vav2 DH with $r^2 = 0.8505$).

titration results were observed when Rac1·mant-GDP-Mg^{2+}, RhoA·mant-GDP-Mg^{2+}, and Cdc42·mant-GDP-Mg^{2+} complexes were titrated with the Vav2 DPC, indicating that titration of all Rho GTPase·GDP-Mg^{2+} complexes studied with Vav2 (both the Vav2 DH and the Vav2 DPC proteins) results in an equilibrium mixture of the Rho GTPase·Vav2 binary complex and free GDP-Mg^{2+}. As shown in Scheme 1, formation of a GTPase·GDP-Mg^{2+}·Vav2 ternary complex

Table 2: Dissociation Constants (μM) of the GTPase·Vav2 Binary Complex[a]

			Rac1					
			wild type	S83A	K116A	K116Q	Cdc42	RhoA
Vav2 DH	I	${}^{app}K_{D(Vav2\ DH-GTPase)}$	49 ± 22	58 ± 16	64 ± 9	65 ± 15	439 ± 136	ND[b]
		${}^{true}K_{D(Vav2\ DH-GTPase)}$	0.09 ± 0.04	0.14 ± 0.04	5.97 ± 0.84	6.28 ± 1.40	3.66 ± 1.13	ND[b]
	II	${}^{app}K_{D(GTPase-GDP)}$	201 ± 32	ND[b]	ND[b]	ND[b]	69 ± 32	0.02 ± 0.01
		${}^{true}K_{D(Vav2\ DH-GTPase)}$	0.09 ± 0.02	ND[b]	ND[b]	ND[b]	1.52 ± 0.70	28.52 ± 19.01
Vav2 DPC	I	${}^{app}K_{D(Vav2\ DPC-GTPase)}$	23 ± 12	26 ± 7	49 ± 16	83 ± 27	694 ± 245	ND[b]
		${}^{true}K_{D(Vav2\ DPC-GTPase)}$	0.04 ± 0.02	0.06 ± 0.02	4.57 ± 1.49	8.14 ± 0.17	5.79 ± 2.04	ND[b]
	II	${}^{app}K_{D(GTPase-GDP)}$	600 ± 220	ND[b]	ND[b]	ND[b]	46.5 ± 16.8	0.03 ± 0.02
		${}^{true}K_{D(Vav2\ DPC-GTPase)}$	0.03 ± 0.01	ND[b]	ND[b]	ND[b]	2.43 ± 0.88	9.82 ± 6.54
Vav2 DPC K533A	I	${}^{app}K_{D(Vav2\ DPC\ K533A-GTPase)}$	94 ± 46	121 ± 38	160 ± 46	128 ± 81	809 ± 93	ND[b]
		${}^{true}K_{D(Vav2\ DPC\ K533A-GTPase)}$	0.17 ± 0.08	0.28 ± 0.09	14.93 ± 4.29	12.56 ± 7.95	6.75 ± 0.78	ND[b]
	II	${}^{app}K_{D(GTPase-GDP)}$	80 ± 10	ND[b]	ND[b]	ND[b]	ND[b]	0.03 ± 0.02
		${}^{true}K_{D(Vav2\ DPC\ K533A-GTPase)}$	0.23 ± 0.03	ND[b]	ND[b]	ND[b]	ND[b]	10.53 ± 7.20

[a] The dissociation constants (μM) were estimated as described in the Supporting Information for Figure 3 (I) and Figure 4 (II), but with different combinations of enzymes (Vav2 DH, Vav2 DPC, and Vav2 DPC K533A) and GTPase substrates (Rac1, Rac1 S83A, Rac1 K116A, Rac1 K116Q, Cdc42, and RhoA). Method I employed mant-GDP-Mg^{2+} fluorescence, which gave apparent K_D values of Vav2 for the various GTPases [${}^{app}K_{D(Vav2-GTPase)}$] (see the Supporting Information). To convert ${}^{app}K_{D(Vav2-GTPase)}$ values to the true K_D values [${}^{true}K_{D(Vav2-GTPase)}$] using eq 6 of the Supporting Information, dissociation constants of GTPases for GDP-Mg^{2+} [${}^{true}K_{D(GTPase-GDP)}$] were measured separately (see the Supporting Information). ${}^{true}K_{D(Rac1-GDP)}$, ${}^{true}K_{D(Rac1\ S83A-GDP)}$, ${}^{true}K_{D(Rac1\ K116A-GDP)}$, ${}^{true}K_{D(Rac1\ K116Q-GDP)}$, ${}^{true}K_{D(Cdc42-GDP)}$, and ${}^{true}K_{D(RhoA-GDP)}$ are 1.8 ± 0.9 μM, 2.4 ± 1.3 μM, 1.4 ± 0.8 mM, 5.2 ± 0.3 mM, 9.1 ± 2.1 μM, and 13 ± 6 μM, respectively. Method II employed GTPase and Vav2 DPC tryptophan fluorescence, which gave apparent K_D values of various GTPases for GDP-Mg^{2+} [${}^{app}K_{D(GTPase-GDP)}$]. Using eq 8 of the Supporting Information in combination with predetermined ${}^{true}K_{D(GTPase-GDP)}$ values, values for ${}^{true}K_{D(Vav2-GTPase)}$ were estimated. Titration of RhoA with Vav2 DH, Vav2 DPC, and Vav2 DPC K533A using method I to obtain ${}^{app}K_{D(Vav2\ DH-GTPase)}$, ${}^{app}K_{D(Vav2\ DPC-GTPase)}$, and ${}^{app}K_{D(Vav2\ DPC\ K533A-GTPase)}$ did not give a saturation binding curve at a Vav2 protein concentration of 20 μM. Therefore, we were not able to obtain reasonable ${}^{app}K_{D(Vav2\ DH-GTPase)}$, ${}^{app}K_{D(Vav2\ DPC-GTPase)}$, and ${}^{app}K_{D(Vav2\ DPC\ K533A-GTPase)}$ values for RhoA employing method I (described in the Supporting Information). The data presented in this table represent results obtained from the best fit ($r^2 > 0.8055$) to a simple hyperbola with the corresponding SD. [b] Not determined.

must occur for catalysis of GNE, yet the lack of detectable GTPase·GDP-Mg^{2+}·Vav2 ternary complex under equilibrium conditions indicates that this ternary complex occurs only transiently. Therefore, the overall enzymatic process is characteristic of the Theorell−Chance mechanism (*28*) wherein the central enzyme−substrate complex is present only transiently. Assuming a Theorell−Chance type mechanism, Scheme 1 can be reduced to Scheme 2, where ${}^{r}k$ represents reduced rate constants. The term [GTPase·GDP-Mg^{2+}]/[GDP-Mg^{2+}] associated with the initial binding step of Vav2 with the GTPase·GDP-Mg^{2+} complex is kinetically competent for the formation of GDP-Mg^{2+}-deficient GTPase (shown as [GTPase]), which includes both the association and dissociation process of GDP-Mg^{2+} to and from GDP-Mg^{2+}-deficient GTPase, respectively, in the presence of Vav2. In Scheme 2, formation of the GTPase·GDP-Mg^{2+}·Vav2 ternary complex is omitted, and only three reduced rate constants (${}^{r}k_{+1}$, ${}^{r}k_{-1}$, and k_{cat}) dominate Vav2-mediated Rho GTPase GNE.

Measurement of Equilibrium Binding Constants of Vav2 for Rho GTPases. According to the Theorell−Chance mechanism (Scheme 2), both Vav2 and GDP-Mg^{2+} compete for the same site of the GTPase; hence, the GTPase cannot bind both GDP-Mg^{2+} and Vav2 at a time in Vav2-mediated Rho GTPase GNE. In this case, ${}^{app}K_D$ of Vav2, determined for each GTPase, must be compensated by the K_D of GDP-Mg^{2+} to determine the true dissociation constant (${}^{true}K_D$) of Vav2 for each GTPase (eq 6 of the Supporting Information). On the basis of the Theorell−Chance-type mechanism, the compensated ${}^{true}K_D$ values in combination with equilibrium kinetic constants (V_{max} and K_M) can provide detailed rate constants (${}^{r}k_{+1}$ with ${}^{r}k_{-1}$ and k_{cat}) for Vav2-mediated Rho GTPase GNE.

Titration of the Rac1·mant-GDP complex with Vav2 DH in the presence of Mg^{2+} gives an apparent dissociation constant of Rac1 for Vav2 DH [${}^{app}K_{D(Vav2\ DH-Rac1)}$] (method I; see the Supporting Information). Accounting for the Theorell−Chance-type mechanism, the binding of Vav2 DH to the GTPase competes with free GDP-Mg^{2+} in solution. Therefore, the ${}^{app}K_{D(Vav2\ DH-Rac1)}$ is compensated by the dissociation constant of GDP-Mg^{2+} for Rac1 [${}^{true}K_{D(Rac1-GDP)}$] by using eq 6 in the Supporting Information to give the true dissociation constant (~90 nM, Table 2) for formation of the Rac1·Vav2 DH complex [${}^{true}K_{D(Vav2\ DH-Rac1)}$]. The ${}^{true}K_{D(Vav2\ DH-Rac1)}$ value determined by method I is in agreement with the value obtained by a tryptophan fluorescence-based reverse titration of the Rac1·Vav2 DH binary complex with GDP in the presence of Mg^{2+} (method II; see the Supporting Information).

Table 2 summarizes the true and apparent dissociation constants for formation of the GTPase·Vav2 complexes [${}^{true}K_{D(Vav2-GTPase)}$ and ${}^{app}K_{D(Vav2-GTPase)}$] measured by methods I and II, and the GTPase·GDP-Mg^{2+} complexes [${}^{app}K_{D(GTPase-GDP)}$ and ${}^{true}K_{D(Vav2-GTPase)}$] (Figures 3 and 4). The results suggest that tight binding interactions between Vav2 DH and the GTPase correlate with the rank order of catalytic efficiency: Rac1 ≫ Cdc42 > RhoA (vide supra).

Comparative Kinetic Analysis of Vav2 Rate Constants for GTPases. As shown in Table 3, detailed rate constants for Vav2 DH-mediated GNE have been estimated. The estimated rate constants are not readily comparable, since ${}^{r}k_{+1}$ (M^{-1} min^{-1}, second-order) is not the same reaction order as ${}^{r}k_{-1}$ (min^{-1}, first-order) and k_{cat} (min^{-1}, first-order). Therefore, a comparison of ${}^{r}k_{+1}$ with ${}^{r}k_{-1}$ and k_{cat} must take into account the substrate concentration of the GTPase (or GDP-Mg^{2+}). When GTPase substrate concentrations are greater than the K_M of the Vav2 DH domain for the GTPase (i.e., >5 μM Rac1), the on-rate of the Vav2 DH domain for the GTPase ([GTPase]${}^{r}k_{+1}$, now first-order) is larger than the k_{cat}, suggesting that k_{cat} is indeed the rate-limiting step. The Vav2 DH domain has larger ${}^{r}k_{+1}$ and k_{cat} values for Rac1 than for Cdc42 and RhoA.

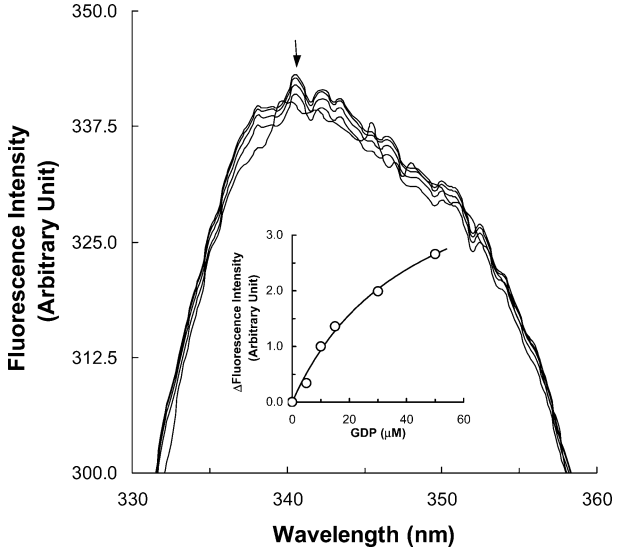

FIGURE 4: Tryptophan fluorescence-based determination of dissociation constants for the Rac1·Vav2 DH binary complex (method II). The Rac1·Vav2 DH binary complex (100 nM) was titrated with unlabeled GDP-Mg^{2+}. Typically, tryptophan is excited at 295 nm, and its maximum emission is observed near 340 nm (*53*). However, since Rayleigh scattering at 295 nm dominates the Rac1 tryptophan emission wavelength at 340 nm, the protein sample was excited at a shorter wavelength (260 mm). While excitation at this wavelength completely removes the Rayleigh scattering interference in the tryptophan emission wavelength at 340 nm, the quantum yields of tryptophan are significantly reduced. Although the change in fluorescence intensity is relatively small, the proportion of the tryptophan fluorescence intensity change is directly dependent on the dissociation of the Vav DH domain from Rac1. Changes in tryptophan fluorescence intensity at 340 nm corresponding to the dissociation of Rac1 from the Vav2 DH domain (as indicated by arrow), due to the binding of GDP-Mg^{2+} to Rac1, were plotted against the titrant GDP-Mg^{2+} concentration (inset). The plot was fit to a simple hyperbola to give ${}^{app}K_{D(Rac1-GDP)}$. The ${}^{app}K_{D(Rac1-GDP)}$ was converted to a ${}^{true}K_{D(Vav2\ DH-Rac1)}$ using eq 8 of the Supporting Information to give a ${}^{true}K_{D(Vav2\ DH-Rac1)}$ of 0.09 ± 0.02 μM Vav2 DH with $r^2 = 0.9065$.

Previous studies have shown that mutation of the PH domain in Vav2 does not affect GEF activity or transforming activity (*17*, *18*). Since the Vav2 DH−PH bidomain is unstable, comparison of the Vav2 DH−PH bidomain reaction kinetics with either the Vav2 DH or Vav2 DPC proteins was not possible. However, the Vav2 DPC domain alone is stable and active; thus, the role of the Vav2 CRD domain was assessed using the Vav2 DPC construct. The presence of the CRD increases the reduced kinetic rates (${}^{r}k_{+1}$, ${}^{r}k_{-1}$, and k_{cat}) for both Cdc42 and RhoA, but the fold increase was smaller than that observed for Rac1 (Table 3). Table 3 also shows that the presence of CRD in the Vav2 DPC predominantly increases the kinetic rates ${}^{r}k_{+1}$ and k_{cat} compared to ${}^{r}k_{-1}$. According to Scheme 2, ${}^{r}k_{+1}$ and k_{cat} represent successful binding interactions of the Vav2 DPC with the GTPase substrate for GTPase GNE, while ${}^{r}k_{-1}$ corresponds to an unproductive kinetic binding process (i.e., dissociation). As noted above, deletion of the PH domain in Vav2 does not affect GEF activity or transforming activity (*17*, *18*). We therefore speculate that the PH domain does not contribute to Vav2 DPC-mediated Rho GTPase GNE. Rather, the CRD domain contained within the Vav2 DPC can enhance GNE of Rho GTPases by the Vav2 DH domain. However, since we cannot assess the true kinetic effect of the Vav2 PH domain on Vav2 DH-mediated Rho GTPase GNE, we cannot eliminate the possible role of the PH domain on Vav2 DH-mediated Rho GTPase GNE. Our data do indicate that the Vav2 CRD mediates favorable association of Vav2 DH with Rho GTPases (${}^{r}k_{+1}$), resulting in an increase in the number of binding interactions between the Vav2 DH domain and GTPase, particularly for the Rac1 GTPase substrate, thereby facilitating GNE. Moreover, in Table 3, we show that the Vav2 DPC K533A mutant drastically reduces ${}^{r}k_{+1}$ for Vav2 DH-mediated Rac1 GNE, consistent with our previous in vivo study (*17*, *18*).

Can the Isolated Vav CRD Couple with the Isolated DH Domain to Enhance Catalysis? To ascertain whether the isolated CRD can act synergistically with the Vav2 DH domain to enhance Rho GTPase GNE, we titrated a mixture of Vav2 DH and Rho GTPase substrate with the Vav1 CRD. Unlike the Vav1 CRD, the Vav2 CRD alone was not stable under our experimental conditions. Therefore, a direct comparison of the effect of the Vav2 CRD and Vav1 CRD, contained within the DPC domain, on the catalytic activity of the Vav2 DH domain for Rho GTPase GNE could not be made. As summarized in Table 4, the isolated Vav1 CRD increases the V_{max} of the Vav2 DH domain for Rac1 and Cdc42 by 1.7- and 1.3-fold, respectively. As in the Vav2 DPC (which contains the DH, PH, and CRD domains in a multidomain fragment of Vav2), where an increase in k_{cat} was observed as compared to that for the Vav2 DH domain alone, the isolated Vav1 CRD can increase the catalytic efficiency of the Vav2 DH domain by increasing the k_{cat}. This result supports our premise that the CRD alters the kinetics of Vav2 DH-mediated Rho GTPase GNE.

The effect of Vav1 CRD-mediated activation on the Vav2 DH domain also appears to be Rac1-specific (Table 4). However, the overall increase in Vav2 DH domain activity due to addition of the isolated Vav1 CRD is approximately 2-fold less than the increase observed for the Vav2 DPC (Table 4). This may be due to an additive effect, in that the extent of formation of the Rac1·GDP-Mg^{2+}·Vav2 DPC ternary complex is greater in the presence of the intact Vav2 DPC protein as opposed to the synergistic effects of the two isolated CRDs and DH domains due to proximity effects. Another possibility is that the Vav1 CRD may not effectively couple with the Vav2 DH domain (as compared to the Vav2 CRD) due to sequence differences between the two Vav isoforms (*40*, *41*). In addition, we cannot eliminate the possibility that the PH domain in the Vav2 DPC has a positive regulatory effect on the binding of Vav2 DH on the GTPase or/and may facilitate interaction of the CRD with the Vav2 DH·GTPase complex, as the Vav1 CRD alone is 2-fold less effective than the Vav2 DPC. Thus, we cannot derive any conclusive results about the role of the PH domain in this study, since we do not have kinetic data on the PH domain and its effect on Vav2 DH-mediated Rho GTPase GNE, as a DH−PH construct could not be stably generated. Further study is required to account for the role of the PH domain in Vav DH-mediated Rho GTPase GNE. Nevertheless, our results indicate that the isolated CRD is able to enhance DH-mediated Rac1 GNE.

Fluorescence Anisotropy and NMR-Based Chemical Shift Mapping Shows that the Vav1 MBP−CRD Protein Associates with Rac1 and RhoA. Like previous GST pull-down experiments performed with the Vav3 CRD and RhoA (*26*), our studies using Vav1 CRD and Vav1 PH−CRD proteins

Table 3: Enzymatic Rate Constants of Vav2 for GTPases[a]

		Rac1					
		wild type	S83A	K116A	K116Q	Cdc42	RhoA
Vav2 DH	${}^{r}k_{+1(\text{Vav2 DH}-\text{GTPase})}$	0.1×10^6	0.2×10^5	658	321	0.3×10^4	359
	${}^{r}k_{-1(\text{Vav2 DH}-\text{GTPase})}$	0.9×10^4	0.3×10^5	0.4×10^4	0.2×10^4	1.2×10^4	0.7×10^4
	$k_{\text{cat(Vav2 DPC}-\text{GTPase})}$	0.6×10^6	0.1×10^6	0.4×10^4	0.3×10^4	3.2×10^4	0.3×10^4
Vav2 DPC	${}^{r}k_{+1(\text{Vav2 DPC}-\text{GTPase})}$	2.5×10^6	0.9×10^5	0.4×10^4	0.3×10^4	1.5×10^4	527
	${}^{r}k_{-1(\text{Vav2 DPC}-\text{GTPase})}$	0.1×10^6	0.5×10^4	1.8×10^4	2.7×10^4	8.7×10^4	0.5×10^4
	$k_{\text{cat(Vav2 DPC}-\text{GTPase})}$	12.9×10^6	0.6×10^6	3.3×10^4	3.0×10^4	8.6×10^4	0.4×10^4
Vav2 DPC K533A	${}^{r}k_{+1(\text{Vav2 DPC K533A}-\text{GTPase})}$	0.3×10^6	0.04×10^6	963	0.2×10^4	0.5×10^4	296
	${}^{r}k_{-1(\text{Vav2 DPC K533A}-\text{GTPase})}$	5.1×10^4	1.1×10^4	0.5×10^6	2.4×10^4	3.5×10^4	0.3×10^4
	$k_{\text{cat(Vav2 DPC K533A}-\text{GTPase})}$	3.8×10^6	0.5×10^6	1.3×10^4	2.2×10^4	6.3×10^4	0.3×10^4

[a] Rate constants ${}^{r}k_{+1}$ (μM^{-1} GDP-Mg^{2+} min^{-1}) and ${}^{r}k_{-1}$ (min^{-1}) are expressed as described by Scheme 2 and were estimated using eqs 11 and 10 of the Supporting Information, respectively. In particular, the ${}^{\text{true}}K_{\text{D(Vav2 DH}-\text{GTPase})}$, ${}^{\text{true}}K_{\text{D(Vav2 DPC}-\text{GTPase})}$, and ${}^{\text{true}}K_{\text{D(Vav2 DPC K533A}-\text{GTPase})}$ values determined by method I (Figure 3) were used for the calculations of all ${}^{r}k_{-1}$ values, except that the ${}^{\text{true}}K_{\text{D(Vav2 DH}-\text{GTPase})}$, ${}^{\text{true}}K_{\text{D(Vav2 DPC}-\text{GTPase})}$, and ${}^{\text{true}}K_{\text{D(Vav2 DPC K533A}-\text{GTPase})}$ values determined by method II (Figure 4) were used for the calculations of RhoA ${}^{r}k_{-1}$ values. The k_{cat} (min^{-1}) values were taken from Table 1. Values of the SD associated with the estimated rate constants obtained from the best fit ($r^2 > 0.7595$) to a simple hyperbola are less than 30% of the values presented here.

Table 4: Effects of the Vav1 CRD on the Vav2 DH Domain-Mediated Guanine Nucleotide Exchange of GTPase[a]

	Rac1					
	wild type	S83A	K116A	K116Q	Cdc42	RhoA
${}^{\text{Vav1 CRD}}V_{\text{max(Vav2 DH}-\text{GTPase})}$	$(0.05 \pm 0.01) \times 10^5$	624 ± 29	ND[b]	180 ± 39	210 ± 65	ND
$V_{\text{max(Vav2 DH}-\text{GTPase})}$[c]	$(0.03 \pm 0.01) \times 10^5$	480 ± 76	21 ± 4	13 ± 6	160 ± 34	14 ± 4
$V_{\text{max(Vav2 DPC}-\text{GTPase})}$[c]	$(0.12 \pm 0.01) \times 10^5$	$(0.03 \pm 0.01) \times 10^5$	163 ± 13	150 ± 3	430 ± 30	19 ± 2
${}^{\text{Vav1 CRD}}V_{\text{max(Vav2 DH}-\text{GTPase})}/V_{\text{max(Vav2 DH}-\text{GTPase})}$	1.7-fold increase	1.3-fold increase	ND	1.2-fold increase	1.3-fold increase	ND
$V_{\text{max(Vav2 DPC}-\text{GTPase})}/V_{\text{max(Vav2 DH}-\text{GTPase})}$	4.0-fold increase	6.3-fold increase	7.8-fold increase	11.5-fold increase	2.7-fold increase	1.4-fold increase
${}^{\text{true}}K_{\text{D(Vav1 CRD}-\text{Vav2 DH}\cdot\text{GTPase}\cdot\text{GDP})}$	0.1 ± 0.0	0.2 ± 0.1	ND	0.2 ± 0.1	0.2 ± 0.2	ND
${}^{\text{true}}K_{\text{D(Vav2 DH}-\text{GTPase})}$[c]	0.09 ± 0.04	0.14 ± 0.04	5.97 ± 0.84	6.28 ± 1.40	3.66 ± 1.13	28.52 ± 19.01
${}^{\text{true}}K_{\text{D(Vav2 DPC}-\text{GTPase})}$[c]	0.04 ± 0.02	0.06 ± 0.02	4.57 ± 1.49	8.14 ± 0.17	5.79 ± 2.04	9.82 ± 6.54

[a] The kinetic values associated with the Vav1 CRD-enhanced maximum activity of the Vav2 DH domain for GTPase substrates [${}^{\text{Vav1 CRD}}V_{\text{max(Vav2 DH}-\text{GTPase})}$] are represented in units of μM GDP$-Mg^{2+}$ min^{-1}, and the true dissociation constants of the Vav1 CRD for the GTPase·GDP-Mg^{2+}·Vav2 DH ternary complex [${}^{\text{true}}K_{\text{D(Vav1 CRD}-\text{Vav2 DH}\cdot\text{GTPase}\cdot\text{GDP})}$] in units of μM GTPase·GDP-Mg^{2+}·Vav2 DH were obtained as described in the Supporting Information. [b] Not determined. [c] For comparison, V_{max} and K_D values associated with the Vav2 DH domain and the Vav2 DPC and their GTPase substrates (Rac1, RhoA, and Cdc42) were taken from Tables 1 and 2. The values presented in this table are the result of the best fit ($r^2 > 0.8095$) to a simple hyperbola with the corresponding SD.

Table 5: Apparent Equilibrium Dissociation Constants for the Interaction of the Vav1 MBP−PH−CRD and Vav1 MBP−CRD Proteins with Rac1 and RhoA GTPases in the Presence and Absence of Mg^{2+} [a]

GTPase·nucleotide (GNP) complex	Mg^{2+}	${}^{\text{Vav1 app}}K_{\text{D(MBP}-\text{PH}-\text{CRD}-\text{GTPase}\cdot\text{GNP})}$	${}^{\text{Vav1 app}}K_{\text{D (MBP}-\text{CRD}-\text{GTPase}\cdot\text{GNP)}}$
Rac1·GDP	no	1.09 ± 0.05	0.32 ± 0.06
	yes	1.80 ± 0.09	1.24 ± 0.07
Rac1·GMPPNP	no	2.03 ± 0.08	1.02 ± 0.06
	yes	3.80 ± 0.21	1.97 ± 0.10
RhoA·GDP	no	1.43 ± 0.13	0.58 ± 0.4
	yes	4.07 ± 0.13	1.82 ± 0.07
RhoA·GMPPNP	no	1.94 ± 0.11	0.82 ± 0.05
	yes	8.15 ± 0.45	4.15 ± 0.16

[a] The concentration of GTPase was 0.2 μM, and the concentration of titrant (Vav1 MBP−PH−CRD or Vav1 MBP−CRD) ranged from 0 to 10 μM. No detectable binding was observed with MBP protein alone which was used as a control. The apparent dissociation constants (μM) associated with Vav1 MBP−PH−CRD [${}^{\text{Vav1 app}}K_{\text{D(MBP}-\text{PH}-\text{CRD}-\text{GTPase}\cdot\text{GNP})}$] and Vav1 MBP−CRD [${}^{\text{Vav1 app}}K_{\text{D(MBP}-\text{CRD}-\text{GTPase}\cdot\text{GNP})}$] for Rac1, RhoA, and Cdc42 GTPases, in the presence and absence of Mg^{2+}, were obtained as described in the Supporting Information. The data presented in this table are the result of the best fit ($r^2 > 0.9540$) to eq 14 with the corresponding SD.

showed that these proteins were capable of binding both Rac1 and RhoA GTPases in "pull-down" assays (data not shown). The ${}^{\text{app}}K_D$ values for the interaction of Vav1 MBP−PH−CRD and MBP−CRD proteins with Rac1 and RhoA were obtained using fluorescence anisotropy, and the results are summarized in Table 5. We assume that the ${}^{\text{app}}K_D$ values presented in Table 5 lie close to the true equilibrium dissociation constant (${}^{\text{true}}K_D$), since no other factors compete or interfere with the binding of the isolated CRD to the Rho GTPases in this assay. The ${}^{\text{app}}K_D$ for binding of the Vav1 MBP−CRD protein to Rac1 was measured using fluorescence anisotropy, fit assuming a single-binding site model, and found to be 1.24 ± 0.07 and 1.97 ± 0.1 μM for the Rac1·GDP-Mg^{2+} and Rac1·GMPPNP·Mg^{2+} complexes, respectively. The association appears to be sensitive to the conformation of the GTPase switch regions as for both Rac1 and RhoA, the Vav1 MBP−CRD protein binds the Rac1·GDP-Mg^{2+} complex preferentially over the Rac1·GMPPNP·

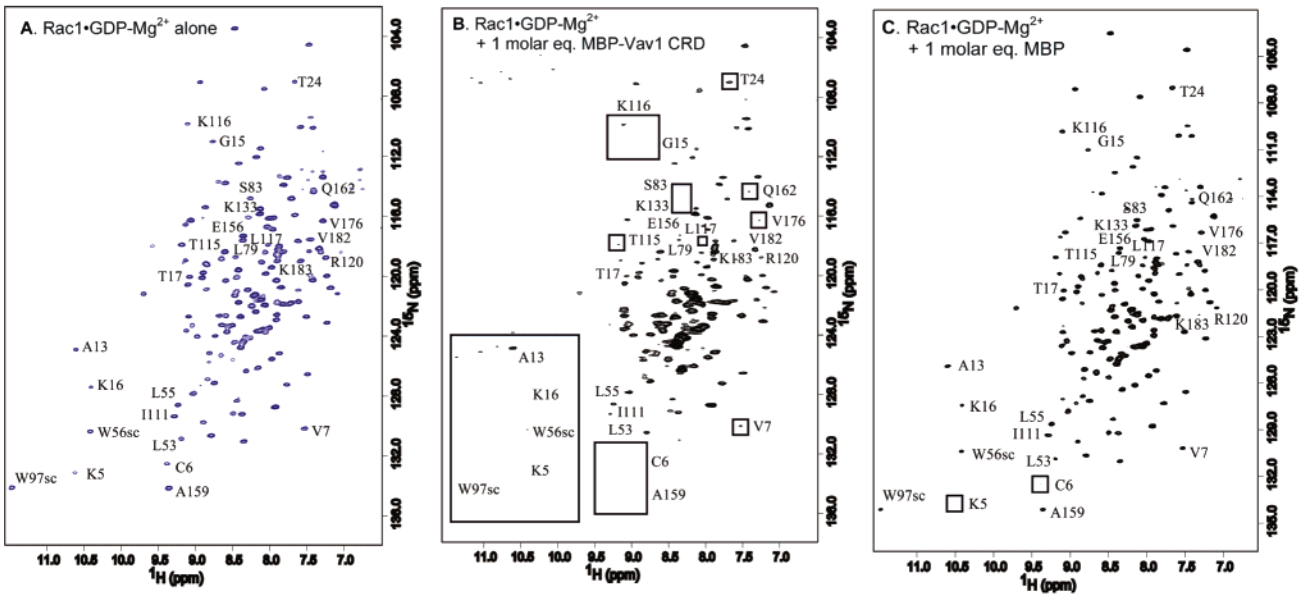

FIGURE 5: Chemical shift mapping studies using NMR. $^{1}H-^{15}N$ HSQC spectra of the Rac1•GDP-Mg^{2+} complex in the absence (A) and presence (B) of the MBP−CRD protein from Vav1 and MBP alone (C) are depicted. Because of the limited solubility of the Vav1 MBP−CRD protein and the inability to express the isolated CRD in *E. coli*, it was necessary to retain the MBP as a solubility enhancement tag. This resulted in an ~70 kDa Rac1•MBP−CRD complex. Residues that disappear from the spectrum in the presence of the MBP−CRD fusion are designated. As expected, no spectral changes are observed in the presence of MBP alone. All spectra were collected at 35 °C and pH 6.8 on an Inova 600 MHz spectrometer.

Mg^{2+} complex. A 2-fold higher $^{app}K_D$ value was obtained for RhoA than for Rac1 in all titrations, indicating that although RhoA is capable of associating with the Vav1 MBP−CRD protein, Rac1 is the preferred GTPase substrate. The MBP−PH−CRD protein had no effect on the overall affinity of the complex, and no detectable binding was observed with MBP alone, suggesting that the observed association can be attributed to the CRD domain.

The anisotropy measurements were confirmed using NMR-based chemical shift mapping studies. The $^{1}H-^{15}N$ TROSY-HSQC spectrum of ^{15}N-labeled Rac1 both free and bound to the Vav1 MBP−CRD protein is shown in Figure 5. Each spectrum shows a single resonance for each amide in the spectrum. The ^{15}N-labeled Rac1•GDP-Mg^{2+} complex was titrated with the unlabeled Vav1 MBP−CRD protein up to a 1:1 molar ratio (data not shown). Given the large size of the complex, the total protein concentration at a 1:1 molar ratio (with 0.25 mM Rac1) is ~18 mg/mL. At these concentrations, the complex is solubility-limited, and thus, it was not possible to increase the protein concentration to a value greater than ~18 mg/mL. At substoichiometric amounts of MBP−CRD, a decrease in peak intensity is observed for a number of cross-peaks in the Rac1 HSQC spectrum and the selective broadening for these Rac1 resonances increases with increasing amounts of the titrant (MBP−CRD) added. Most of the remaining cross-peaks remain unchanged in chemical shift (Figure 5A−C), although a small increase in the overall amide $^{1}H_N$ and ^{15}N line widths is observed for all resonances due to the increase in the molecular mass of the complex. The selective broadening of Rac1 resonances suggests that only a subset of resonances are distributed between the bound and free environments such that the chemical shift difference between the two forms of the protein is approximately equal to the rate of exchange between the two sites. Therefore, residues that are either directly or indirectly affected by complex formation with the MBP−CRD protein display "intermediate exchange" behavior on the NMR time scale, and the disappearance of residues from the Rac1 HSQC spectrum is a result of the chemical exchange behavior of these residues rather than an increase in the molecular mass of the complex (~68 kDa), which would cause uniform broadening for all residues in the protein. Rac1 residues that are perturbed due to the addition of the Vav1 CRD include residues in β-strand 1 (K5, C6, and V7), loop 1 (A13, G15, K16, and T17) α-helix 1 (Y23 and T24), β-strand 3 (L53, G54, and L55), loop 2 (Y64, S71, and Y72), β-strand 4 (S83), α-helix 3 (V93, R94, and A95), β-strand 5 (I110, I111, L112, V113, G114, K116, and T118), and α-helix 5 (S178 and A159) and the indole side chains of W56 and W97. Intriguingly, many of these Rac1 residues cluster near the guanine base in the nucleotide-binding pocket (Figure 6). No spectral changes are observed in the presence of MBP alone; therefore, the disappearance of cross-peaks in the Vav1 CRD•GDP-Mg^{2+}•Rac1 spectrum is attributed to a specific interaction between Rac1 and the Vav1 CRD.

Chemical shift mapping using NMR spectroscopy is a tool commonly used to identify binding surfaces on proteins. However, since ligand-induced chemical shift perturbations can result from both direct and remote changes in the protein's chemical or electronic environment, extrapolation of binding interactions from chemical shift changes needs to be interpreted with caution. The analysis of NMR chemical shift data is often simplified when information about the total magnitude of perturbations is available. However, the intermediate exchange behavior of the complex, as in the case of the Vav1 CRD•GDP-Mg^{2+}•Rac1 complex, prevents quantification of chemical shift data. In such cases, NMR chemical shift mapping data can be combined with information from previous structural and mutagenesis results to aid in identification of binding sites. To identify a contiguous binding interface on Rac1 for the Vav1 CRD, we mapped

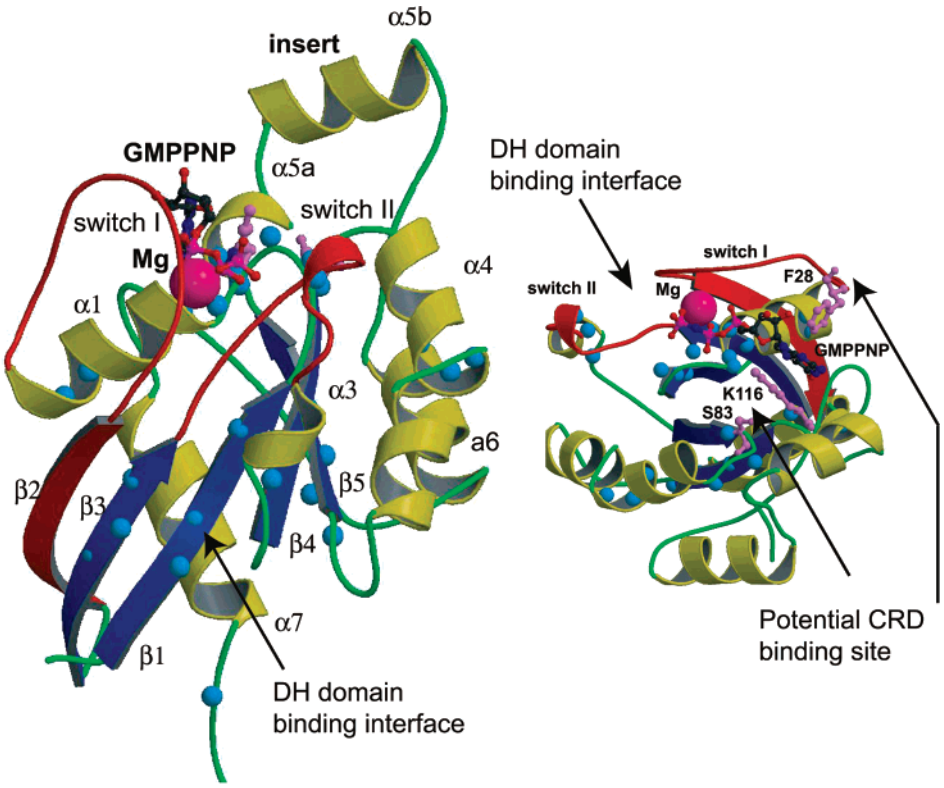

FIGURE 6: Residues sensitive to the presence of the Vav1 MBP−CRD protein are mapped on the Rac1·GMPPNP structure. Backbone amides that are perturbed in the presence of the Vav1 MBP−CRD protein are highlighted in blue on the Rac1·GMPPNP crystal structure (PDB entry 1MH1). The GMPPNP nucleotide is shown in ball-and-stick format, and the side chains of K116, F28, and S83 are colored violet. The switch regions are colored red. The $\beta1-\beta2-\beta3$ face and the switch regions near the bound magnesium form the binding interface for the DH domain of Rho GEFs. A second potential binding surface for the CRD is identified from NMR studies that either lies in the proximity of the K116−S83 binding interface or indirectly perturbs this region by binding near switch 1.

the perturbed Rac1 residues onto the Rac1·GMPPNP crystal structure (*42*) (Figure 6). Two contiguous surfaces could be identified. The first surface consists of residues in the first three β-strands, and in the switch regions (switch I and switch II) of Rac1 which comprise part of the binding interface with the DH domain of the Rho GEFs Tiam-1 and Dbs (*10*, *11*). In particular, Rac-1 residues K5, W56, Y64, and S71, associated with this surface, make direct contacts with the DH domain in the crystal structure of the Rac1/Tiam-1 DH−PH complex. The second surface consists of residues that do not form the DH domain interface and lie in loop 1, β-strands 4 and 5, and α-helix 5.

The NMR solution structure of the Vav1 DH domain (*25*) shows that many of residues in the Vav1 DH domain (such as E201, T205, Q331, K335, L338, N371, and E372) that are expected to interact with the GTPase are conserved in sequence and in the conformation of their side chains, suggesting a similar mode of GTPase recognition for the Vav1 DH domain as is observed for Tiam-1 and Dbs. Given the sequence and structural conservation of the recognition interfaces between the DH domain of Vav and other Rho GEF family members, the Vav DH domain is predicted to interact with residues associated with the first contiguous surface on Rac1 identified by NMR. Although it is possible that the CRD- and DH-binding surfaces overlap, we focused on the second surface, as these residues lie outside regions of direct interaction with the DH domain and thus may be involved in Vav CRD binding. This second surface consists of basic, polar, and hydrophobic residues: K116, S83, G12, A13, Y64, R94, and A95. These residues lie in a solvent-exposed binding cleft formed by β-strands 4 and 5 and lie in the proximity of the bound nucleotide (Figure 6).

Identification of Residues outside the Known DH Domain-Binding Interface on Rac1. Among the Rac1 residues that comprise the second contiguous surface, residue K116 is particularly intriguing. K116 is highly conserved in most Ras family GTPases and is part of the NKXD motif that is important for coordinating the guanine base (*42*). The side chain of K116 appears to stabilize the nucleotide-binding pocket by stacking against the guanine base, and forming hydrogen bonding interactions with the ribose oxygen and the backbone carbonyl of A13 in the Rac1·GMPPNP (PDB entry 1MH1) and RhoA·GTPγS (PDB entry 1FTN) crystal structures (*42*, *43*). The crystal structures of Cdc42 in various nucleotide-bound forms (PDB entry 1A4R) show that whereas Q116 also packs against the guanine base, its interactions in the nucleotide-binding pocket are not as extensive as that of the corresponding lysine in Rac1 and RhoA (*42*, *43*). Cdc42, TC10, and TTF are the only Rho GTPases in which K116 is replaced with a glutamine (*44*).

In H-Ras, the N116I, K117E, and D119N mutants are considered to be dominant negatives (*45*, *46*), and all three mutants have been shown to inhibit SDC25C- or Cdc25-mediated GNE (*45*, *46*). It has been proposed that inhibition of Ras GNE is due to formation of a catalytically inactive complex between these mutants and the Ras GEF. The kinetic importance of this residue in Rho proteins has also been illustrated for Rac1, RhoA, and Cdc42 (*42*−*44*). Although K116 is a glutamine in Cdc42, mutation of Q116 to lysine in Cdc42 has been reported to completely abolish

Cdc24-mediated nucleotide exchange (*47*). Recently, Heo and Meyer (*48*) have identified several switch-of-function mutants for Rac1 and Cdc42 based upon the ability of these mutants to induce morphology changes in vivo (*48*). Intriguingly, K116 scored as the single most important specificity-defining switch-of-function residue in Rac1. In addition, using single-point mutations and deletion mutagenesis, Movilla and Bustelo (*49*) have proposed that the region near strand β_5 and K118 in RhoA (K116 in Rac1) is sensitive to Vav3-mediated GNE (*49*). Given the observations described above and results from our chemical shift mapping experiments, we characterized the effect of K116A and mutations on Vav2 DH- and DPC-mediated GNE. Since mutation of K116 is also expected to alter the intrinsic exchange rate of dissociation of the bound nucleotide, we also mutated S83 of Rac1 to an alanine. S83 lies in the proximity of K116 in the Rac1 tertiary structure. However, since S83 does not directly contact the nucleotide, and the S83 side chain is at least partially solvent exposed, mutation of this residue was not expected to affect the intrinsic rate of GDP dissociation in Rac1.

In addition, previous studies on Vav2 CRD mutants showed that Vav2 CRD residues K533, K538, and V568 are critical for Vav2 function in vivo (*17*). Mutation of K533 to alanine significantly inhibited both Vav2 transformation and signaling and reduced GNE activity, although a rigorous kinetic analysis was not previously performed. A homology model of Vav2 (Figure 2) built using the CRD of PKCδ as a template shows that K533 is expected to be solvent-exposed and lies in a loop (between strands β1 and β2) that in most typical CRDs is important for binding DAG and lipid ligands. In the protein kinase C-δ CRD, the loop between strands β1 and β2 is involved in interactions with the PKC activator, phorbol ester, and may be involved in plasma membrane insertion (*50*). The $\beta1-\beta2$ region is quite divergent in the Vav1 CRD, and given the role of the Vav1 and Vav2 CRDs in membrane association, it is possible that the Vav CRD has diverged from other members of the typical CRD family such as protein kinase C to recognize more divergent lipid second messengers such as a phosphoinositides, or GTPase substrates. Nevertheless, mutation of this residue to alanine is not expected to affect the overall structure of the Vav2 CRD, although it does affect Vav2 function.

Kinetic Analyses of Rac1 and Vav Mutants. Kinetic results, as summarized in Table 3, show that replacement of S83 of Rac1 with alanine and K116 with an alanine or glutamine decreases ${}^{r}k_{+1}$ and k_{cat}, but not ${}^{r}k_{-1}$, for Vav2 DH-mediated Rac1 GNE. The observed perturbation of these kinetic rates is CRD-independent, since the Vav2 DH construct lacks the CRD. Moreover, when the CRD is present in the Vav2 protein (i.e., Vav2 DPC), a greater decrease in ${}^{r}k_{+1}$ and k_{cat} for the Rac1 S83A and K116A/Q variants is observed (Table 3). The presence of the CRD in the Vav2 DPC domain enhances ${}^{r}k_{+1}$ and k_{cat} relative to those of the Vav2 DH domain for wild-type Rac1 GNE ~25- and 21-fold [${}^{r}k_{+1(\text{Vav2 DPC}-\text{Rac1})}/{}^{r}k_{+1(\text{Vav2 DH}-\text{Rac1})} = 2.5 \times 10^6/0.1 \times 10^6 = 25$ and $k_{cat(\text{Vav2 DPC}-\text{Rac1})}/k_{cat(\text{Vav2 DH}-\text{Rac1})} = 12.9 \times 10^6/0.6 \times 10^6 = 21$], respectively. In contrast, only 10- and 12-fold decreases in ${}^{r}k_{+1}$ and k_{cat} [${}^{r}k_{+1(\text{Vav2 DPC}-\text{Rac1 K116Q})}/{}^{r}k_{+1(\text{Vav2 DH}-\text{Rac1 K116Q})} = 3333/321 = \sim 10$ and $k_{cat(\text{Vav2 DPC}-\text{Rac1 K116Q})}/k_{cat(\text{Vav2 DH}-\text{Rac1 K116Q})} = 30000/2600 = \sim 12$] are observed for the Rac1 K116Q variant (Table 3). Similar observations were made for K116A and S83A mutants, suggesting that residues S83 and K116 are sensitive to the association of the Vav2 DH domain with Rac1 via the CRD.

These kinetic results suggest that the Rac1 region encompassing S83 and K116 is involved in catalytic binding interactions between Rac1 and the Vav DH domain as well as the Vav CRD, and thereby mutations at these positions discourage the catalytic processes of ${}^{r}k_{+1}$ and k_{cat}. On the basis of our NMR, kinetic, and structural analyses, we propose that binding of the Vav DH domain to the Rac1 region, including S83 and K116, may alter the Rac1 GDP binding interactions to increase ${}^{r}k_{+1}$ and k_{cat}. Additional binding of the Vav CRD on, or near, the same site further increases ${}^{r}k_{+1}$ and k_{cat}, resulting in facilitation of Rac1 GNE. It is possible that the increase in catalytic steps ${}^{r}k_{+1}$ and k_{cat} upon binding of the Vav DH domain to Rac1 is due to a conformational change in the Rac1 region of S83 and K116 that couples with the conformational changes in the Ras nucleotide-binding pocket. Additional binding interactions with the Vav CRD may further facilitate conformational changes in Rac1 (i.e., region containing S83 and K116), which propagate to the Ras nucleotide-binding pocket, resulting in the enhancement of the Vav DH-mediated Rac1 GNE.

Our kinetic studies also show that mutation of K533 to alanine in the Vav2 DPC impairs the initial binding interaction (${}^{r}k_{+1}$) of Vav2 toward Rac1 (Table 3). Other rate constants of Vav2 DPC K533A-mediated Rac1 GNE (${}^{r}k_{-1}$ and k_{cat}) were not significantly altered (Table 3). Similar results were observed for Cdc42 and RhoA (Table 3). Therefore, Vav2 CRD residue K533 plays an important role in modulating the initial association (${}^{r}k_{+1}$) between the Vav2 DH domain and the GTPase substrate, but is dispensable for the subsequent steps in the enzymatic process.

Kinetic analysis of the interaction of the Vav2 DPC K533A variant with Rac1 mutants S83A, K116A, and K116Q was also examined (Table 3). As for the effect of the Vav2 DPC K533A mutant on Vav2 DH domain activity toward wild-type Rac1, the Vav2 DPC K533A variant did not enhance the ${}^{r}k_{+1}$ of Rac1 variants S83A and K116A/Q by the Vav2 DH domain (Table 3). Thus, the modulation of Vav2 DH domain activity for Rac1 GNE by CRD residue K533 may be independent of Rac1 residues K116 and S83.

DISCUSSION

In this study, we have investigated the detailed catalytic mechanism associated with both the DH domain and CRD of Vav on Rho GTPase-mediated GNE. We show that the enzymatic process of Vav-mediated GNE for Rho GTPases is likely to proceed via a Theorell−Chance mechanism, in which the ternary complex is only transiently populated during the enzymatic process (*28*). Our observation is consistent with the previous studies of Ras GTPase−Cdc25 interactions, in that the Cdc25^{Mm285}·GDP-Mg^{2+}·Ras ternary complex was not observed when the Ras·GDP-Mg^{2+} complex was titrated with the Ras GEF core domain, Cdc25^{Mm285} (*39*).

Numerous biological and biochemical studies have determined that the DH domain of Vav1 and Vav2 can function as a GEF for Rac1, RhoA, and Cdc42 in vitro and in vivo (*18*, *19*, *32*, *33*). Vav DH domain transforming activity has

previously been attributed to activation of Rac1 in vivo (*32*, *51*), although these data conflict with a recent report (*52*) showing that Vav-mediated transformation is a complex process that involves activation of RhoA, Rac1, and Cdc42 GTPases in addition to NF-κB and MAPK (*52*). Our kinetic studies on the minimal DH domain of Vav2 show that outside the cellular milieu, Vav2 is an active GEF toward all three Rho GTPases, RhoA, Rac1, and Cdc42. However, whereas values for the "unproductive" initial binding rate constant ($^{r}k_{-1}$) are not significantly different for Rac1, RhoA, and Cdc42, the "successful" binding interactions (combination of $^{r}k_{+1}$ and k_{cat}) for Vav2 DH-mediated GNE are vastly different for the three GTPases studied: Rac1 $\gg$ Cdc42 $>$ RhoA. These results suggest that at least for the minimal DH unit, in the absence of phosphoinositides and phosphorylation, Rac1 is the preferred substrate.

The Vav CRD is known to be a positive modulator of Vav2 DH activity and has sequence determinants that are important for membrane targeting and GTPase recognition, thereby enhancing the transforming activity of onco-Vav (*17*). Previous studies have shown that some residues of the CRD severely impair Vav2 DH activity as well as Vav protein-mediated cellular signaling (*16*, *17*). Our kinetic studies show that the presence of the Vav2 CRD in Vav2 DPC increases the $^{r}k_{+1}$ and k_{cat} values for Vav2 DH-mediated Rac1 GNE, suggesting that the CRD plays an active role in the enzymatic process of Vav2 DH-mediated GNE of Rac1 by enhancing successful binding interactions between Vav2 DH and Rac1, but not by simply serving as an accessory binding domain for Vav2 DH domain−GTPase interactions.

Our NMR spectroscopic studies and fluorescence anisotropy measurements show that the Vav1 CRD can directly associate with both Rac1 and RhoA. In particular, $^{1}H-^{15}N$ HSQC spectra of Rac1 show that of a number of Rac1 residues, including S83 and K116, which are proximal to the guanine base are perturbed by an addition of the Vav1 CRD. When Rac1 residues S83 and K116 were replaced with other amino acids (e.g., alanine), no significant increase in $^{r}k_{+1}$ and k_{cat} in the presence of the CRD (Vav DPC) was observed. These results suggest that the CRD-mediated enhancement of Vav2 DH domain catalytic activity on Rac1 GNE is attributed to direct association of the Vav CRD with Rac1. Residues S83 and K116 that lie near the Rac1 nucleotide-binding pocket may form part of this interface or be indirectly perturbed in response to CRD binding.

In addition, we have shown that Vav2 CRD residue K533 is important for Rac1 association, and this facilitates Vav2 DH-mediated GNE of Rac1. Detailed kinetic analyses of the Vav2 DPC K533A CRD variant for Rac1 GNE presented in this study show that Vav2 CRD residue K533 may be involved in the initial binding interaction (represented by $^{r}k_{+1}$) of the Vav2 DPC with Rho GTPase substrates, since the Vav2 DPC K533A mutant decreases the $^{r}k_{+1}$ only for wild-type Rac1, Rac1 variants (S83A and K116A/Q), and Cdc42 and RhoA. Therefore, our results suggest that Vav2 CRD residue K533 is important for association of Vav2 with Rac1 in a manner independent of the effects mediated by Rac1 residues S83 and K116.

In conclusion, this study supports a Theorell−Chance-type mechanism of Vav DH domain-catalyzed Rho GTPase GNE. Moreover, the initial binding event and the rate-limiting k_{cat} step of the Vav DH domain for its GTPase substrate determine the in vitro catalytic specificity of the Vav DH domain toward the Rho GTPases, Rac1, RhoA, and Cdc42. This study also shows that the Vav CRD promotes successful binding interactions ($^{r}k_{+1}$ and k_{cat}) between the Vav DH domain and Rac1 and thus regulates Vav DH domain-mediated Rac1 GNE. Rac1 residues S83 and K116 may serve as modulatory sites.

ACKNOWLEDGMENT

We thank MinQi Lu for the purification of GTPases, the Vav1 MBP−CRD protein, and Vav2 protein domains. We thank Dr. Thomas Darden for help with Amber minimization of the Vav2 CRD homology model.

SUPPORTING INFORMATION AVAILABLE

Methods for the (i) determination of GTPase binding constants for GDP-Mg^{2+}, (ii) fluorescence-based kinetics of Vav2-mediated GTPase GNE, (iii) determination of binding constants for the GTPase·Vav2 binary complex (methods I and II), (iv) estimation of Vav2 rate constants for GTPases, (v) equilibrium titration of the Vav2 DH domain and GTPase with the Vav1 CRD, (vi) fluorescence anisotropy measurements, and (vii) molecular modeling. This material is available free of charge via the Internet at http://pubs.acs.org.

REFERENCES

1. Burridge, K., and Wennerberg, K. (2004) Rho and Rac take center stage, *Cell 116*, 167−179.
2. Zohn, I. M., Campbell, S. L., Khosravi-Far, R., Rossman, K. L., and Der, C. J. (1998) Rho family proteins and Ras transformation: The RHOad less traveled gets congested, *Oncogene 17*, 1415−1438.
3. Etienne-Manneville, S., and Hall, A. (2002) Rho GTPases in cell biology, *Nature 420*, 629−635.
4. Hoffman, G. R., and Cerione, R. A. (2002) Signaling to the Rho GTPases: Networking with the DH domain, *FEBS Lett. 20*, 85−91.
5. Van Aelst, L., and D'Souza-Schorey, C. (1997) Rho GTPases and signaling networks, *Genes Dev. 11*, 2295−2322.
6. D'Souza-Schorey, C., Boshans, R. L., McDonough, M., Stahl, P. D., and Van Aelst, L. (1997) A role for POR1, a Rac1-interacting protein, in ARF6-mediated cytoskeletal rearrangements, *EMBO J. 16*, 5445−5454.
7. Whitehead, I. P., Campbell, S. L., Rossman, K. L., and Der, C. J. (1997) Dbl family proteins, *Biochim. Biophys. Acta 1332*, F1−F23.
8. Erickson, J. W., and Cerione, R. A. (2004) Structural elements, mechanism, and evolutionary convergence of Rho protein-guanine nucleotide exchange factor complexes, *Biochemistry 43*, 837−842.
9. Cerione, R. A., and Zheng, Y. (1996) The Dbl family of oncogenes, *Curr. Opin. Cell Biol. 2*, 216−222.
10. Worthylake, D. K., Rossman, K. L., and Sondek, J. (2000) Crystal structure of Rac1 in complex with the guanine nucleotide exchange region of Tiam1, *Nature 408*, 682−688.
11. Rossman, K. L., Worthylake, D. K., Snyder, J. T., Siderovski, D. P., Campbell, S. L., and Sondek, J. (2002) A crystallographic view of interactions between Dbs and Cdc42: PH domain-assisted guanine nucleotide exchange, *EMBO J. 21*, 1315−1326.
12. Snyder, J. T., Worthylake, D. K., Rossman, K. L., Betts, L., Pruitt, W. M., Siderovski, D. P., Der, C. J., and Sondek, J. (2002) Structural basis for the selective activation of Rho GTPases by Dbl exchange factors, *Nat. Struct. Biol. 9*, 468−475.
13. Karnoub, A. E., Worthylake, D. K., Rossman, K. L., Pruitt, W. M., Campbell, S. L., Sondek, J., and Der, C. J. (2001) Molecular basis for Rac1 recognition by guanine nucleotide exchange factors, *Nat. Struct. Biol. 8*, 1037−1041.
14. Gao, Y., Xing, J., Streuli, M., Leto, T. L., and Zheng, Y. (2001) Trp(56) of rac1 specifies interaction with a subset of guanine nucleotide exchange factors, *J. Biol. Chem. 276*, 47530−47541.

15. Zhu, K., Debreceni, B., Li, R., and Zheng, Y. (2000) Identification of Rho GTPase-dependent sites in the Dbl homology domain of oncogenic Dbl that are required for transformation, *J. Biol. Chem. 275*, 25993−26001.
16. Palmby, T. R., Abe, K., and Der, C. J. (2002) Critical role of the pleckstrin homology and cysteine-rich domains in Vav signaling and transforming activity, *J. Biol. Chem. 277*, 39350−39359.
17. Booden, M. A., Campbell, S. L., and Der, C. J. (2002) Critical but distinct roles for the pleckstrin homology and cysteine-rich domains as positive modulators of Vav2 signaling and transformation, *Mol. Cell. Biol. 22*, 2487−2497.
18. Abe, K., Rossman, K. L., Liu, B., Ritola, K. D., Chiang, D., Campbell, S. L., Burridge, K., and Der, C. J. (2000) Vav2 Is an Activator of Cdc42, Rac1, and RhoA, *J. Biol. Chem. 275*, 10141−10149.
19. Liu, B. P., and Burridge, K. (2000) Vav2 activates Rac1, Cdc42, and RhoA downstream from growth factor receptors but not β1 integrins, *Mol. Cell. Biol. 20*, 7160−7169.
20. Cerione, R. A., and Zheng, Y. (1996) The Dbl family of oncogenes, *Curr. Opin. Cell Biol. 8*, 216−222.
21. Han, J., Luby-Phelps, K., Das, B., Shu, X., Xia, Y., Mosteller, R. D., Krishna, U. M., Falck, J. R., White, M. A., and Broek, D. (1998) Role of substrates and products of PI 3-kinase in regulating activation of Rac-related guanosine triphosphatases by Vav, *Science 279*, 558−560.
22. Bradford, M. M. (1976) A Rapid and Sensitive Method for the Quantitation of Microgram Quantities of Protein Utilizing the Principle of Protein-Dye Binding, *Anal. Biochem. 72*, 248−254.
23. Mott, H. R., Carpenter, J. W., Zhong, S., Ghosh, S., Bell, R. M., and Campbell, S. L. (1996) The solution structure of the Raf-1 cysteine-rich domain: A novel ras and phospholipid binding site, *Proc. Natl. Acad. Sci. U.S.A. 93*, 8312−8317.
24. Hommel, U., Zurini, M., and Luyten, M. (1994) Solution structure of a cysteine rich domain of rat protein kinase C, *Nat. Struct. Biol. 1*, 383−387.
25. Aghazadeh, B., Lowry, W. E., Huang, X. Y., and Rosen, M. K. (2000) Structural basis for relief of autoinhibition of the Dbl homology domain of proto-oncogene Vav by tyrosine phosphorylation, *Cell 102*, 625−633.
26. Movilla, N., and Bustelo, X. R. (1999) Biological and regulatory properties of Vav-3, a new member of the Vav family of oncoproteins, *Mol. Cell. Biol. 19*, 7870−7885.
27. Segel, I. H. (1976) *Biochemical calculations*, 2nd ed., John Wiley & Sons, New York.
28. Segel, I. H. (1993) *Enzyme kinetics*, Wiley-Interscience, New York.
29. Campbell, S. L., Khosravi-Far, R., Rossman, K. L., Clark, G. J., and Der, C. J. (1998) Increasing complexity of Ras signaling, *Oncogene 17*, 1395−1413.
30. Reinstein, J., Schlichting, I., Frech, M., Goody, R. S., and Wittinghofer, A. (1991) p21 with a phenylalanine 28 → leucine mutation reacts normally with the GTPase activating protein GAP but nevertheless has transforming properties, *J. Biol. Chem. 266*, 17700−17706.
31. Thapar, R., Moore, C. D., and Campbell, S. L. (2003) Backbone ^{1}H, ^{13}C, and ^{15}N resonance assignments for the 21 kDa GTPase Rac1 complexed to GDP and Mg^{2+}, *J. Biomol. NMR 27*, 87−88.
32. Crespo, P., Schuebel, K. E., Ostrom, A. A., Gutkind, J. S., and Bustelo, X. R. (1997) Phosphotyrosine-dependent activation of Rac-1 GDP/GTP exchange by the vav proto-oncogene product, *Nature 385*, 169−172.
33. Olson, M. F., Pasteris, N. G., Gorski, J. L., and Hall, A. (1996) Faciogenital dysplasia protein (FGD1) and Vav, two related proteins required for normal embryonic development, are upstream regulators of Rho GTPases, *Curr. Biol. 6*, 1628−1633.
34. Koshland, D. E. (2002) The application and usefulness of the ratio k_{cat}/K_M, *Bioorg. Chem. 30*, 211−213.
35. Nassar, N., Hoffman, G. R., Manor, D., Clardy, J. C., and Cerione, R. A. (1998) Structures of Cdc42 bound to the active and catalytically compromised forms of Cdc42GAP, *Nat. Struct. Biol. 5*, 1047−1052.
36. Zhang, B., Zhang, Y., Wang, Z., and Zheng, Y. (2000) The role of Mg^{2+} cofactor in the guanine nucleotide exchange and GTP hydrolysis reactions of Rho family GTP-binding proteins, *J. Biol. Chem. 275*, 25299−25307.
37. Shutes, A., Phillips, R. A., Corrie, J. E., and Webb, M. R. (2002) Role of magnesium in nucleotide exchange on the small G protein rac investigated using novel fluorescent guanine nucleotide analogues, *Biochemistry 41*, 3828−3835.
38. Shimizu, T., Ihara, K., Maesaki, R., Kuroda, S., Kaibuchi, K., and Hakoshima, T. (2000) An open conformation of switch I revealed by the crystal structure of a Mg^{2+}-free form of RHOA complexed with GDP. Implications for the GDP/GTP exchange mechanism, *J. Biol. Chem. 275*, 18311−18317.
39. Lenzen, C., Cool, R. H., Prinz, H., Kuhlmann, J., and Wittinghofer, A. (1998) Kinetic Analysis by Fluorescence of the Interaction between Ras and the Catalytic Domain of the Guanine Nucleotide Exchange Factor $Cdc25^{Mm}$, *Biochemistry 37*, 7420−7430.
40. Henske, E. P., Short, M. P., Jozwiak, S., Bovey, C. M., Ramlakhan, S., Haines, J. L., and Kwiatkowski, D. J. (1995) Identification of VAV2 on 9q34 and its exclusion as the tuberous sclerosis gene TSC1, *Ann. Hum. Genet. 59*, 25−37.
41. Schuebel, K. E., Bustelo, X. R., Nielsen, D. A., Song, B. J., Barbacid, M., Goldman, D., and Lee, I. J. (1996) Isolation and characterization of murine vav2, a member of the vav family of proto-oncogenes, *Oncogene 13*, 363−371.
42. Hirshberg, M., Stockley, R. W., Dodson, G., and Webb, M. R. (1997) The crystal structure of human rac1, a member of the rho-family complexed with a GTP analogue, *Nat. Struct. Biol. 4*, 147−152.
43. Wei, Y., Zhang, Y., Derewenda, U., Liu, X., Minor, W., Nakamoto, R. K., Somlyo, A. V., Somlyo, A. P., and Derewenda, Z. S. (1997) Crystal structure of RhoA-GDP and its functional implications, *Nat. Struct. Biol. 4*, 699−703.
44. Rudolph, M. G., Wittinghofer, A., and Vetter, I. R. (1999) Nucleotide binding to the G12V-mutant of Cdc42 investigated by X-ray diffraction and fluorescence spectroscopy: Two different nucleotide states in one crystal, *Protein Sci. 8*, 778−787.
45. Hwang, Y. W., Zhong, J. M., Poullet, P., and Parmeggiani, A. (1993) Inhibition of SDC25 C-domain-induced guanine-nucleotide exchange by guanine ring binding domain mutants of v-H-ras, *J. Biol. Chem. 268*, 24692−24698.
46. Cool, R. H., Schmidt, G., Lenzen, C. U., Prinz, H., Vogt, D., and Wittinghofer, A. (1999) The Ras mutant D119N is both dominant negative and activated, *Mol. Cell. Biol. 19*, 6297−6305.
47. Li, R., and Zheng, Y. (1997) Residues of the Rho family GTPases Rho and Cdc42 that specify sensitivity to Dbl-like guanine nucleotide exchange factors, *J. Biol. Chem. 272*, 4671−4679.
48. Heo, W. D., and Meyer, T. (2003) Switch-of-function mutants based on morphology classification of Ras superfamily small GTPases, *Cell 113*, 315−328.
49. Movilla, N., Dosil, M., Zheng, Y., and Bustelo, X. R. (2001) How Vav proteins discriminate the GTPases Rac1 and RhoA from Cdc42, *Oncogene 20*, 8057−8065.
50. Zhang, G., Kazanietz, M. G., Blumberg, P. M., and Hurley, J. H. (1995) Crystal structure of the cys2 activator-binding domain of protein kinase C delta in complex with phorbol ester, *Cell 81*, 917−924.
51. Crespo, P., Bustelo, X. R., Aaronson, D. S., Coso, O. A., Lopez-Barahona, M., Barbacid, M., and Gutkind, J. S. (1996) Rac-1 dependent stimulation of the JNK/SAPK signaling pathway by Vav, *Oncogene 13*, 455−460.
52. Palmby, T. R., Abe, K., Karnoub, A. E., and Der, C. J. (2004) Vav transformation requires activation of multiple GTPases and regulation of gene expression, *Mol. Cancer Res. 2*, 702−711.
53. Campbell, I. D., and Dwek, R. A. (1984) *Biological Spectroscopy*, The Benjamin/Cummings Publishing Co., Menlo Park, CA.

BI047443Q